J. Phys. Chem. A **2004,** *108,* 7347−7355

Simulations of the Vibrational Relaxation of a Model Diatomic Molecule in a Nanoconfined Polar Solvent

Shenmin Li,[†] Tricia D. Shepherd,[‡] and Ward H. Thompson*,[†]

Department of Chemistry, University of Kansas, Lawrence, Kansas 66045-7582, and Department of Chemistry/ Physics, Westminster College, Salt Lake City, Utah 84105

Received: April 14, 2004; In Final Form: June 25, 2004

The vibrational dynamics of a model diatomic anion solute dissolved in a methyl iodide solvent confined in a nanoscale spherical cavity are investigated by molecular dynamics simulations. The effect of confining the solvent on the vibrational energy relaxation time T_1, solvent-induced frequency shift $\langle\delta\omega\rangle$, and pure dephasing time T_2^* is examined by comparing the results from confined systems of varying size (cavity radius 0.8−2 nm) to those from the bulk system. It is found that T_1 increases monotonically toward the bulk solvent value with increasing cavity size, and good agreement is found between equilibrium molecular dynamics simulations based on perturbation theory and classical nonequilibrium dynamics simulations. In contrast to T_1, the solvent-induced frequency shift and the dephasing time do not change monotonically with cavity size. The results are discussed in terms of the changes in solvent structure and dynamics due to confinement.

1. Introduction

The structure and dynamics of confined liquids have attracted increasing attention in recent years.[1−14] The confinement of liquids in microporous media, such as sol−gels, zeolites, supramolecular assemblies, and reverse micelles, can lead to dramatic changes in their static and dynamical properties from those of the bulk system.[15] A number of experimental approaches have been used to probe these changes including steady-state absorption and fluorescence spectra,[16−33] time-dependent fluorescence,[16−33] NMR spectroscopy,[1,34−37] OKE spectroscopy,[38−43] dielectric relaxation spectroscopy,[44,45] charge-transfer reactions,[46,47] Raman spectroscopy,[2,3,9,10,48] and infrared pump−probe experiments.[6,7] Taken together these experiments can access equilibrium and nonequilibrium structure and dynamics including processes dominated by long- and short-range interactions. Among these, the vibrational dynamics investigated by Raman spectra and time-resolved vibrational pump−probe experiments have been comparatively less well-studied. The results of these measurements are vibrational frequency shifts ($\langle\delta\omega\rangle$), dephasing times ($T_2^*$), and energy relaxation times (T_1), processes in which the solvent−solute short-range repulsive interactions play a large role. Thus, they provide a valuable complement to measurements that are sensitive to the longer-range electrostatic interactions (e.g., optical spectra); these quantities also each probe slightly different solvent properties and solute−solvent interactions. In addition, they are a useful starting point for well-controlled studies of energy transfer across nanoscale interfaces, a topic of increasing interest. In this paper we investigate the vibrational dynamics in a nanoconfined solvent by calculating $\langle\delta\omega\rangle$, T_2^*, and T_1 by molecular dynamics simulations.

Recently, Zhong et al. have studied vibrational energy relaxation (VER) of pseudohalide ions, N_3^-, NCO^-, and NCS^- confined in nanoscale water pools inside nonionic reverse micelles (RMs) by ultrafast infrared spectroscopy.[6,7] These three systems all gave similar results as a function of the RM water pool radius; i.e., the VER times are about three times longer for the smallest RM studied than the values measured for bulk water, and become shorter with increasing RM size (but do not reach the bulk value for the largest RM studied). The solvent-induced frequency redshift was also observed to decrease toward the value in bulk water as the RM size was increased.[5] However, the magnitudes of the frequency shifts are much different for various solutes or even the same solute in different micelles. For instance, the redshifts for NCS^- are much smaller than those for NCO^- and N_3^-. The redshift is less than one wavenumber for NCS^- in bulk H_2O but in nonionic RMs it is 7−8 cm^{-1}. Zhong et al. qualitatively explained the longer VER times and solvent-induced redshifts in terms of “the reduced interactions between the ions and solvent” which is ultimately related to the water−surfactant interactions.[7]

Interestingly, several groups[1−3,9,10,48,49] have measured the vibrational dephasing time, T_2, of neat, nonaqueous solvents in sol−gels and found a different trend. Specifically, Jonas and co-workers found that T_2 becomes shorter with decreasing pore size (in fact, $T_2^{-1} \propto 1/R_{\text{cav}}$), and the solvent induces a frequency blueshift. The accelerated vibrational dephasing upon confinement was attributed to an increase in the orientational order relative to the bulk liquid and to liquid-surface interactions. Tominaga et al. obtained similar results.[49] Both groups explained their observations in terms of a two-state model in which liquid molecules inside the pore are classified into “surface molecules” and “bulk molecules”.[1,48,49]

These experimental results indicate some of the possible interesting vibrational dynamics occurring in confined solvents and demonstrate the sensitivity to the characteristics of the confining framework. However, there has been little theoretical study of confinement effects on vibrational dynamics.[4,50−52] In this paper, we investigate the vibrational dynamics in a simple model system of a solute dissolved in a nanoconfined solvent. The emphasis here is on developing a general understanding of the origins of the trends in $\langle\delta\omega\rangle$, T_2^*, and T_1 for a simple model system. The present work is not intended as a realistic simulation

---

[†] University of Kansas.

[‡] Westminster College.

10.1021/jp048361e CCC: \$27.50

of a system studied experimentally, which will be a focus of future work. Thus, the solute is taken to be a model diatomic anion (AB^-), and the solvent is dipolar, non-hydrogen bonding CH_3I. In this initial study we choose a confinement framework that is relatively inert: a rigid, hydrophobic spherical cavity that can have, at best, a limited participation in the vibrational dynamics. This serves two purposes: (1) it allows for comparisons with previous simulations of steady-state absorption and fluorescence spectra[4] and time-dependent fluorescence measurements, and (2) it provides a useful reference point for investigating the role of the surface. The vibrational energy relaxation time, solvent-induced frequency shift, and pure dephasing time are calculated for spherical cavities of varying size by equilibrium molecular dynamics simulations (EMD) and compared to the values in the bulk system. As an important validation step, nonequilibrium molecular dynamics simulations (NEMD) are also used to calculate the VER time.

The rest of this paper is organized as follows. In section II, we describe the basic theory of vibrational energy relaxation and vibrational dephasing. A brief discussion of the method used for computing the numerical Fourier transform is also given in this section. The details of the computational model and procedures are given in section III. The calculated results are presented and possible vibrational relaxation mechanisms in the confined system are discussed in section IV. Finally, the main conclusions are summarized in section V.

II. Theoretical Background

A. Vibrational Energy Relaxation. 1. Equilibrium Molecular Dynamics (EMD). The most prevalent approach for calculating the vibrational energy relaxation time T_1 is based on perturbation theory[53−55]

$$T_1 = \frac{\mu k_B T}{\xi(\omega_0)} \tag{1}$$

where μ is the reduced mass of the solute molecule, k_B is Boltzmann's constant, T is the temperature, and $\xi(\omega_0)$ is the power spectrum of the force−force time correlation function, $\langle \delta F_1(t) \delta F_1(0) \rangle$, at the solute vibrational frequency ω_0:

$$\xi(\omega_0) = \int_0^\infty \cos(\omega_0 t) \langle \delta F_1(t) \delta F_1(0) \rangle \, dt \tag{2}$$

Here

$$F_1 = \mu \left[\frac{\vec{F}_B}{m_A} - \frac{\vec{F}_A}{m_B} \right] \cdot \hat{r}_{AB} + \frac{L^2}{I r_e} \tag{3}$$

where $\vec{F}_A$ and $\vec{F}_B$ denote the total forces on the A and B atoms, respectively, $\hat{r}_{AB}$ is the unit vector from A to B, L is the solute angular momentum, I is the of moment of inertia, and r_e is the equilibrium AB bond distance. Thus, $\delta F_1(t)$ is the fluctuation of the force F_1 exerted by solvent atoms and solute rotation along the solute bond at time t. In principle, the force TCF should be evaluated quantum mechanically. However, since this is computationally unfeasible for a many-body real system, the classical force TCF is usually used and a correction factor is introduced to account for quantum effects.[56−59] The classical TCF can be easily obtained from the EMD simulations, by monitoring the fluctuations of force F_1 at each MD time step.

There are well-known issues concerning the accuracy of the EMD approach for calculating T_1. The first is how to deal with the Fourier transform of the force-force time correlation function (TCF), particularly for a solute with a high vibrational frequency. The second is how to properly account for quantum effects, which has focused attention on the calculation of quantum correction factors (QCFs) to the classical force TCF. Two kinds of techniques are widely used to perform the Fourier transform. One is fitting the force TCF to an analytic function from which an analytic Fourier transform form can be obtained.[60,61] This method is usually used for short-time fitting and therefore is primarily applicable when the force TCF decays quickly. The other is performing the Fourier transform numerically. However, the traditional fast Fourier transform can suffer from numerical noise for solutes with high vibrational frequency.[62,63] In this paper, we use the modified Hurwitz−Zweifel (MHZ) method[64,65] to calculate the cosine Fourier integral in eq 2 numerically. This method was adopted to calculate the VER time of I_2 in a xenon solvent and yielded satisfactory results.[62] With regard to the QCFs,[56−59] we do not use them in our calculations for two reasons: (1) there is not an obvious form of the QCF to use for an arbitrary liquid system,[59] and (2) our interest is in the confinement effect on T_1 and there is not yet a clear method for estimating the dependence of the quantum correction to the VER time on the confined system size.

The MHZ approach, presented by Thakkar and Smith,[65] is to subdivide the range and integrate between the successive zeros of $\cos(\omega_0 t)$, thus converting the infinite integral to a summation of terms C_n, which is referred to as the Hurwitz−Zweifel expansion.[64] The Clenshaw-Curtis quadrature method[66] is used here to evaluate the C_n as suggested by Thakkar and Smith.[65] The main difficulty is that the C_n series may converge slowly. To accelerate the convergence, a reliable and fairly general scheme is to use the van Wijngaarden modification of the Euler transformation.[67] The details of the numerical evaluation procedures can be found in reference 65.

2. Nonequilibrium Molecular Dynamics (NEMD). Nonequilibrium molecular dynamics can be used to determine classical vibrational energy relaxation times directly by investigating the time decay of excess vibrational energy. If the energy decay is exponential, the relaxation time T_1 is given by

$$\frac{\langle E_v(t) \rangle - \langle E_v(\infty) \rangle}{\langle E_v(0) \rangle - \langle E_v(\infty) \rangle} = e^{-t/T_1} \tag{4}$$

where $\langle E_\nu(t) \rangle$ is the nonequilibrium average of the vibrational energy for a diatomic solute at time t, and $\langle E_\nu(\infty) \rangle$ and $\langle E_\nu(0) \rangle$ are the equilibrium average vibrational energy and the nonequilibrium average initial energy, respectively. The solute vibrational energy at time t is monitored in a nonequilibrium trajectory such as

$$E_v(t) = \frac{{p_r}^2(t)}{2\mu} + V[r(t)] \tag{5}$$

where r is the solute anion bond distance with conjugate momentum p_r, and $V(r)$ is the solute potential energy.

B. Vibrational Dephasing and Frequency Shifts. Theoretical treatments have show that the dephasing time T_2 and VER time T_1 are related by[68]

$$\frac{1}{T_2} = \frac{1}{2T_1} + \frac{1}{T_2^*} \tag{6}$$

where T_2^* is the pure dephasing time. It is generally the case in a liquid that T_1 is comparatively long and makes a negligible contribution to the overall vibrational dephasing time T_2. Therefore, in many cases the spectral line width is a measure of the pure dephasing time T_2^* only.[2,3] According to the Kubo theory[69−71] of dephasing, the pure dephasing time T_2^* is given by

$$\frac{1}{T_2^*} = \int_0^\infty \langle \delta\omega(0)\delta\omega(t)\rangle \, \mathrm{d}t \tag{7}$$

where $\langle \delta\omega(0)\delta\omega(t)\rangle$ is the time correlation function of solvent-induced vibrational frequency shift, $\delta\omega(t) = \omega(t) - \langle\omega\rangle$. A widely used method for calculating $\delta\omega(t)$ in EMD simulations was introduced by Oxtoby.[72] Using time-independent perturbation theory and considering only the first excited state, the frequency shift can be described by a linear term ($\delta\omega_1$) and a quadratic term ($\delta\omega_2$)

$$\delta\omega(t) = \delta\omega_1(t) + \delta\omega_2(t) \tag{8}$$

with

$$\delta\omega_1(t) = (Q_{11} - Q_{00})F_1(t) \tag{9}$$

$$\delta\omega_2(t) = [(Q^2)_{11} - (Q^2)_{00}]F_2(t) \tag{10}$$

Here, $F_1(t)$ is the force defined in eq 3 while $F_2(t)$ is half the derivative of $F_1(t)$ with respect to the solute vibrational coordinate displacement, $Q = r - r_e$, evaluated at $Q = 0$. In this work, $F_2(t)$ is calculated numerically during the equilibrium MD simulation. The expectation values Q_{11}, Q_{00}, $(Q^2)_{11}$, and $(Q^2)_{00}$ are calculated by solving the stationary Schrödinger equation of the isolated solute molecule, $\hat{H}\psi = E\psi$, where the Hamiltonian has the form

$$\hat{H} = \frac{\hat{p}_\mu^{\,2}}{2\mu} + \hat{V}(Q) \tag{11}$$

and the diatomic potential V is taken to be a Morse function. In addition, for a rigid solute diatomic molecule, the vibration−rotation coupling contribution to the frequency shift can be split as in eq 8[73]

$$\delta\omega_{\mathrm{rot}}(t) = \delta\omega_{r1}(t) + \delta\omega_{r2}(t) \tag{12}$$

with

$$\delta\omega_{r1}(t) = -(Q_{11} - Q_{00})\frac{L^2(t)}{Ir_e} \tag{13}$$

$$\delta\omega_{r2}(t) = 3[(Q^2)_{11} - (Q^2)_{00}]\frac{L^2(t)}{2Ir_e^{\,2}} \tag{14}$$

where $L(t)$ is the solute angular momentum at time t, and since $\langle L^2\rangle/2I = kT$, this gives

$$\langle\delta\omega_{\mathrm{rot}}\rangle = \left\{-2\frac{(Q_{11} - Q_{00})}{r_e} + 3\frac{(Q^2)_{11} - (Q^2)_{00}}{r_e^{\,2}}\right\}kT \tag{15}$$

This implies that within perturbation theory the frequency shift induced by solute vibration−rotation coupling is independent of the surroundings.

III. Model and Simulation Details

Molecular dynamics simulations are carried out to investigate the vibrational dynamics of one solute AB$^-$ anion in a CH$_3$I solvent confined in spherical cavities of varying size. The corresponding results for the bulk system are also presented. All simulations are carried out at an average temperature of 298 K and a solvent density of 2.0 g/cm^3. For simulations of confined solvents, the cavity radius is chosen to be 8, 10, 12, 15, and 20 Å; the corresponding numbers of solvent molecules at this density are given in Table 2. For simulations of the bulk system, the minimum image convention and periodic boundary conditions are used, with 107 CH$_3$I molecules in a cubic box of length 23.29 Å.

TABLE 1: Potential Parameters[a]

site	ϵ(kcal/mol)	σ(Å)	q	r$_{ij}$	mass (g/mol)
		Solute			
A	0.1195	3.0	−1.2		15
B	0.1195	3.0	+0.2	1.2	15
		Solvent			
CH$_3$	0.2378	3.77	+0.25		15
I	0.5985	3.83	−0.25	2.16	126.8
		Cavity Wall			
	0.46	2.5	0.0		

[a] Morse parameters for AB bond: $D_e = 7$ ev; $\beta = 1.2$ Å^{-1}.

TABLE 2: Vibrational Energy Relaxation Time T_1, Dephasing Time T_2*, and Number of Solvent Molecules vs Cavity Size and for the Bulk System

	$R_{\mathrm{cav}} =$ 8 Å	$R_{\mathrm{cav}} =$ 10 Å	$R_{\mathrm{cav}} =$ 12 Å	$R_{\mathrm{cav}} =$ 15 Å	$R_{\mathrm{cav}} =$ 20 Å	bulk
T_1-EMD† (ps)[a]	47.0	54.0	58.7	61.1	62.9	82.3
T_1-EMD (ps)	33.5	44.3	46.9	51.9	53.0	63.5
T_1−NEMD (ps)	37.0	39.5	43.0	48.6	49.1	63.5
T_2^* (ps)	0.80	0.04	0.13	0.51	0.71	3.67
no. of solvent molecules	11	24	44	92	234	107

[a] T_1-EMD† denotes the VER time obtained by EMD simulation without the solute vibration−rotation coupling contribution.

The form of the interaction potential is the same as in our previous work.[4] The potential parameters are given in Table 1. For the confined system, the potential functions are a sum of Coulomb, $u_C(r_{ij})$, and Lennard-Jones, $u_{LJ}(r_{ij})$, interactions for all pairs of sites and molecule−wall interaction terms, $u_w(r_i)$, for all sites:

$$U = \sum_{i<j} u_C(r_{ij}) + \sum_{i<j} u_{LJ}(r_{ij}) + \sum_i u_w(r_i) \tag{16}$$

with

$$u_C(r_{ij}) = \frac{q_i q_j}{r_{ij}} \tag{17}$$

$$u_{LJ}(r_{ij}) = 4\epsilon_{ij}\left[\left(\frac{\sigma_{ij}}{r_{ij}}\right)^{12} - \left(\frac{\sigma_{ij}}{r_{ij}}\right)^{6}\right] \tag{18}$$

Here r_{ij} is the distance between sites i and j in two different molecules, and q_i and q_j are the fixed charges on sites i and j. The interactions of the liquid with the cavity walls, u_w, is the 9−3 potential (with curvature corrections) developed by Linse and Halle.[74,75] The potential depends only on the radial distance of site i from the center of cavity. The parameters for u_w are the same as in ref 8 (see Table 1). For the bulk system, only Coulomb and Lennard-Jones terms are involved and the Ewald summation procedure[76] has been used to describe the long-range Coulomb interactions.

In this paper, the diatomic solute anion AB$^-$ is chosen as a two-site model with equal masses and site charges of $q_A = -1.2$ and $q_B = 0.2$ (see Table 1). The AB$^-$ bond is held rigid in the EMD simulations while a flexible AB$^-$ bond described by a Morse potential is used in the NEMD simulations; the same

Morse potential is also used in the calculation of the solvent-induced frequency shift. The two-site rigid model for CH_3I of Freitas et al. is used for the solvent molecules.[77] Since the primary goal of this work is to investigate the fundamental effects of confinement on vibrational dynamics rather than simulate a specific experimental system, we have not included a positive counterion in the present calculations. A counterion may very well affect all of the observables studied here ($\langle \delta\omega \rangle$, T_2*, and T_1); we plan to investigate this in the near future. However, we have chosen to neglect the counterion in these simulations to keep the system as simple as possible.

The AB^- vibrational frequency is chosen to be $\omega_0 = 800$ cm^{-1}. This frequency is somewhat small compared to real molecules with similar atomic masses. It is used for three reasons: (1) there is larger numerical noise in performing the Fourier transform for a solute with a higher vibrational frequency, (2) for this particular system, if the solute frequency is larger than 1000 cm^{-1}, the VER time will be longer than 1 ns, therefore the computational expense for the NEMD simulation will be dramatically increased, and (3) this ω_0 is high enough compared to the characteristic frequencies of solvent that a possible solute−solvent resonant energy transfer is avoided.[78,79]

The constant temperature ensemble (*NVT*) is used during the EMD simulations with the temperature maintained at a mean value of 298 K by a Nose−Hoover thermostat.[80,81] The force exerted along the AB^- bond by the solvent atoms as well as the solute rotation is monitored at each MD time step from which the force TCF is computed. The dynamic friction evaluated at the gas-phase vibrational frequency ($\omega_0 = 800$ cm^{-1}) is obtained by the MHZ method. To obtain converged results, an ensemble average of 10 trajectories (each 3 ns long with a stepsize of 1 fs) is used.

For the NEMD simulations, an anharmonic (Morse) solute model is used with an initial excitation energy of $\Delta E_0 = 1200$ cm^{-1}, corresponding to the vibrational energy of the AB^- anion in the $n = 1$ excited-state including zero point energy. A trajectory is first propagated for a 50 ps equilibration period (*NVT*, $T = 298$ K). Then the solute vibrational energy is increased by ΔE_0 from the average equilibrium vibrational energy of k_BT. All excess energy is added as kinetic energy by setting the bond distance to the equilibrium value. Next, a 200 ps constant energy ensemble (NVE) nonequilibrium trajectory is run for data collection. An additional 30 ps *NVT* equilibration period is performed before another nonequilibrium trajectory is run. This procedure is repeated for a total of 250 trajectories with a stepsize of 1 fs. Both the EMD and NEMD simulations are carried out based on the DLPOLY molecular dynamics simulation package.[82]

IV. Results and Discussion

A. Vibrational Energy Relaxation Time. The calculated VER times of the AB^- solute in CH_3I confined in spherical cavities of varying size (and in bulk solvent) obtained using the EMD and NEMD simulations are listed in Table 2 and plotted in Figure 1. A number of features are worth noting: (1) The VER time T_1 increases monotonically as the cavity size increases. This is in contrast to the results of Zhong et al. who observed a monotonic decrease in T_1 with increasing cavity size.[6,7] (2) The relaxation time, T_1, increases by ~60% (~33%) from the smallest to the largest cavity in the EMD (NEMD) simulations. (3) The bulk limit is still not reached for the largest cavity, $R_{cav} = 20$ Å. This result is not surprising if we look at the solvent radial density distribution for the cavity systems in Figure 2 (see below). (4) The EMD results including the solute vibration−rotation coupling contribution are in excellent agreement with the NEMD simulations. (Note that the vibration−rotation coupling is included implicitly in the NEMD simulations.)

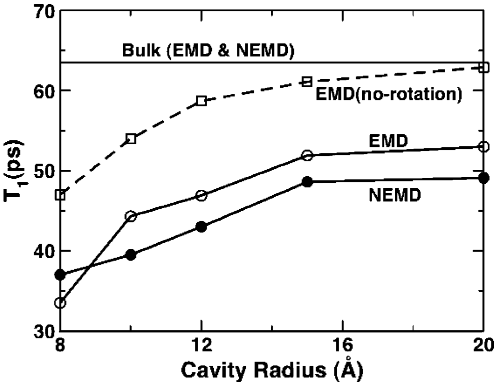

Figure 1. Vibrational energy relaxation time T_1 plotted as a function of cavity radius. Results obtained by NEMD simulations (filled-circles, solid line), EMD simulations (open circles, solid line), and EMD simulations without the vibration−rotation coupling (open squares, dashed line). For comparison, the value for the bulk system is plotted (thin solid line). Note that the NEMD and full EMD simulations give the same value for the bulk system.

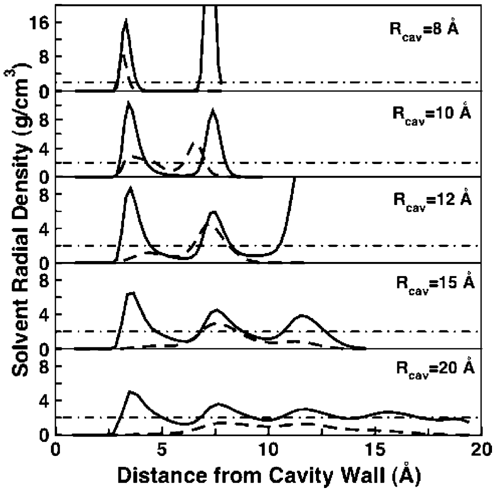

Figure 2. Solvent density and solute probability distribution are shown vs center-of-mass distance from the cavity wall for cavities of varying size. The global solvent density (2.0 g/cm^3) is plotted as a dot−dashed line. Solid lines show the solvent radial density distributions, while dashed lines show the solute probability distributions. To make the overlap of the two distributions clear, the solute distribution is magnified 10 times except for the smallest cavity system, for which it is magnified 4 times.

As noted above the local solvent density distributions plotted in Figure 2 have a significant effect on the vibrational relaxation. A layered solvent structure is observed that is related to the cavity size as has been seen in previous studies.[4,8,11] As illustrated in Figure 2 there are 2, 2, 3, 3, and 4 solvent layers, respectively, for the five cavity radii of 8, 10, 12, 15, and 20 Å. The peak density of the solvent layer nearest the cavity wall is higher than that of the inside layer except for two special cases, the layers located in the center of the 8 and 12 Å cavities. These two high-density peaks are due to a single solvent molecule located (by the center-of-mass) in the center of cavity. (The small volumes of the histogram bins nearest the cavity center give the extremely large densities.) Comparing the solvent layer nearest the wall for different cavity systems we find that the local solvent density increases dramatically as cavity size decreases. For the smallest cavity ($R_{\rm cav} = 8$ Å), the peak value of solvent density is ~16 g/cm^3, eight times the average solvent density. For the largest cavity ($R_{\rm cav} = 20$ Å), the peak density is ~4.5 g/cm^3, more than twice the 2.0 g/cm^3 average solvent density.

To further clarify the confinement effect on vibrational relaxation dynamics, we plot the solute probability distributions (dashed lines in Figure 2) with the solvent radial densities. The biggest region of overlap of the solute distribution and solvent density moves from the solvent layer nearest the wall to the inner layers with increasing cavity size. Nearly complete overlap occurs in the outermost layer for the smallest cavity system, while the overlap is located between two solvent layers for $R_{\rm cav} = 10$ Å. For $R_{\rm cav} = 12$ and 15 Å, the solute is primarily found in the second solvent layer with smaller population in the first and third layers. The solute probability is evenly distributed in the second and third solvent layers for the biggest cavity ($R_{\rm cav} = 20$ Å). Thus, the solute anion is located in the outermost, higher density solvent layer for a smaller cavity system; as the cavity size increases, the solute position shifts toward the cavity center where the solvent densities are somewhat lower. This is consistent with T_1 decreasing with decreasing cavity size since the solute is located in increasingly higher density solvent layers leading to faster vibrational energy relaxation.

B. Force—Force Time Correlation Function (TCF). Within the perturbation theory approximation, eq 1, the vibrational relaxation time T_1 is directly related to the Fourier transform of the force-force time correlation function. It is useful to analyze this TCF to obtain mechanistic information. The unnormalized and normalized force TCFs for cavities of varying sizes, along with the bulk system, are plotted in Figure 3. The force TCF exhibits a fast decay in less than 0.1 ps followed by a long-time decay. Except for the smallest cavity, the static contribution, $|\langle F_1(0)\rangle|^2$, and the magnitude of the long-time tail both increase with decreasing cavity size. In addition, the normalized force TCF in Figure 3b indicates that the fast decay process is similar for both confined and bulk systems, while the slow decay process is quite dependent on cavity size.

To study the various components of the force TCF contributions to the VER time, we decompose the total TCF into three terms corresponding to contributions from the interaction potential (subscript V), solute vibration—rotation coupling (subscript R), and the cross term (subscript V—R):

$$\langle \delta F_1(t)\delta F_1(0)\rangle = \langle \delta F_1(t)\delta F_1(0)\rangle_{\rm V} + \langle \delta F_1(t)\delta F_1(0)\rangle_{\rm R} + 2\langle \delta F_1(t)\delta F_1(0)\rangle_{\rm V-R} \quad (19)$$

The potential term $\langle \delta F_1(t)\delta F_1(0)\rangle_{\rm V}$ can be further decomposed into the contributions from different interactions (including cross terms) according to the interaction potential described by eq 16,

$$\langle \delta F_1(t)\delta F_1(0)\rangle_{\rm V} = \langle \delta F_1(t)\delta F_1(0)\rangle_{\rm C} + \langle \delta F_1(t)\delta F_1(0)\rangle_{\rm LJ} + \langle \delta F_1(t)\delta F_1(0)\rangle_{\rm w} + 2\langle \delta F_1(t)\delta F_1(0)\rangle_{\rm C-LJ} + 2\langle \delta F_1(t)\delta F_1(0)\rangle_{\rm C-w} + 2\langle \delta F_1(t)\delta F_1(0)\rangle_{\rm LJ-w} \quad (20)$$

The time dependence of the total force TCF and its decompositions for cavities with $R_{\rm cav} = 8$ and 15 Å are shown in Figures 4 and 5, respectively. Except for the smallest cavity system, the components of the force TCF due to the cavity wall (including cross-correlations) are insignificantly small. Therefore, only the Coulomb term, Lennard-Jones term and their cross term are shown in Figure 5. Note that only the results for $R_{\rm cav} = 15$ Å system are shown since the TCF and its decompositions for other confined systems (except $R_{\rm cav} = 8$ Å) and the bulk are quite similar in pattern.

It is clear from Figures 4 and 5 that the biggest contribution to the force TCF is from the Lennard-Jones interactions. The contribution due to the Coulombic interactions is less than half

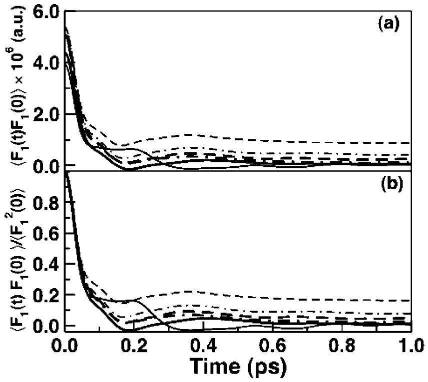

Figure 3. (a) Unnormalized and (b) normalized force-force time correlation functions for the confined cavity systems of varying size and the bulk system are plotted vs time. Results are shown for cavity systems with $R_{\rm cav} = 8$ Å (thin solid line), 10 Å (thin dashed lines), 12 Å (thin dot—dashed line), 15 Å (thick dashed line), and 20 Å (thick dot—dashed line) and the bulk system (thick solid line).

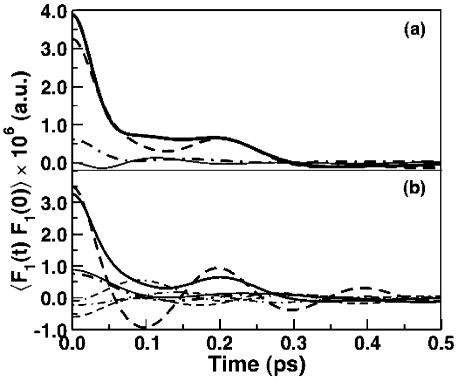

Figure 4. Plot of contributions of the different interaction terms to the force autocorrelation function for $R_{\rm cav} = 8$ Å. Shown in panel a are the total TCF (thick solid line) and the potential (dashed line), vibration—rotation coupling (dash—dotted line), and cross term (thin solid line) contributions. In panel b, the potential (thick solid line), Lennard-Jones (thick dashed line), Coulomb (thick dash—dotted line), and cavity wall (thin solid line) interaction contributions are shown along with the Lennard-Jones—Coulomb (thin dashed line), Lennard-Jones—wall (thin dash—dotted line), and Coulomb—wall (dot—dash-dashed line) cross terms.

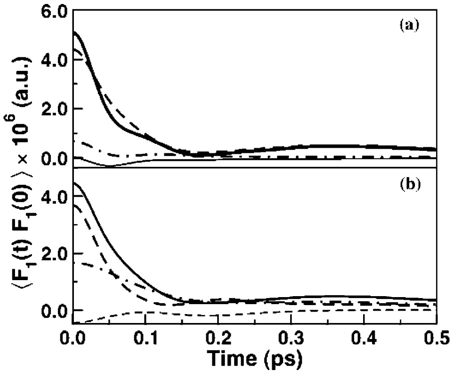

Figure 5. Same as Figure 4 except for $R_{\rm cav} = 15$ Å. In panel b contributions and cross terms related due to the cavity wall interactions are small and not shown.

TABLE 3: Frequency Shifts (in cm^{-1}) of AB$^-$ in CH$_3$I Solvent Confined in Spherical Cavities of Varying Size and the Bulk along with the Different Contributions[a]

	$R_{cav} = 8$ Å	$R_{cav} = 10$ Å	$R_{cav} = 12$ Å	$R_{cav} = 15$ Å	$R_{cav} = 20$ Å	bulk
$\langle\delta\omega\rangle$	13.79(23)	3.74(65)	5.31(26)	5.61(25)	5.57(13)	2.91(10)
$\langle\delta\omega_1\rangle$	−0.60(14)	−6.30(51)	−4.73(21)	−4.30(20)	−4.20(19)	−5.81(10)
$\langle\delta\omega_2\rangle$	14.38(9)	10.04(17)	10.03(8)	9.91(6)	9.78(6)	8.72(8)
$\langle\delta\omega_r\rangle$	−0.73(1)	−0.75(1)	−0.76(1)	−0.76(1)	−0.76(1)	−0.77(2)
$\langle\delta\omega_{r1}\rangle$	−3.15(3)	−3.20(5)	−3.27(2)	−3.27(3)	−3.27(3)	−3.29(10)
$\langle\delta\omega_{r2}\rangle$	2.41(3)	2.45(4)	2.51(2)	2.49(2)	2.50(2)	2.52(7)
$\langle\delta\omega_C\rangle$	−17.49(7)	−14.64(22)	−13.48(16)	−13.06(15)	−12.74(7)	−12.54(6)
$\langle\delta\omega_{C1}\rangle$	−18.11(7)	−15.44(23)	−14.16(16)	−13.70(15)	−13.36(7)	−13.10(6)
$\langle\delta\omega_{C2}\rangle$	0.61(1)	0.80(2)	0.68(1)	0.64(1)	0.62(1)	0.56(1)
$\langle\delta\omega_{LJ}\rangle$	24.22(16)	18.43(61)	19.47(21)	19.42(19)	19.08(13)	16.22(9)
$\langle\delta\omega_{LJ1}\rangle$	15.81(11)	11.92(40)	12.66(14)	12.65(13)	12.42(8)	10.59(6)
$\langle\delta\omega_{LJ2}\rangle$	8.41(5)	6.52(21)	6.81(7)	6.78(6)	6.65(5)	5.64(3)
$\langle\delta\omega_w\rangle$	7.79(14)	0.69(11)	0.09(6)	0.01(1)	0.00(1)	
$\langle\delta\omega_{w1}\rangle$	4.84(9)	0.41(7)	0.05(3)	0.00(1)	0.00(1)	
$\langle\delta\omega_{w2}\rangle$	2.94(5)	0.28(4)	0.04(2)	0.01(1)	0.00(1)	

[a] Data in parentheses are the uncertainty in the mean value with 95% confidence limit.[85]

of the Lennard-Jones term, however it is nearly canceled by the Coulomb−Lennard-Jones cross term as was found in previous studies.[83] Thus, the net *direct* contribution from Coulomb forces is very small.

Comparing the force correlation functions shown for $R_{cav} = 8$ and 15 Å in Figures 4 and 5, respectively, the biggest difference is the Lennard-Jones term. For the $R_{cav} = 8$ Å cavity, the small number of molecules gives a less liquidlike environment for the solute. As a result, significant coherence is present (as strong oscillations) in the force TCFs plotted in Figure 4, particularly for the Lennard-Jones contribution. In addition, the solute−cavity wall interactions contribute significantly to the total TCF for this cavity. However, with increasing cavity size, the contribution from the cavity wall becomes small and the solute environment is much more like a liquid, if an inhomogeneous one. This is reflected in the Lennard-Jones correlation decay that is rapid and smooth (Figure 5).

Finally, we examine different components of the TCF in the frequency domain (power spectra of TCF) obtained by the MHZ method. The results for $R_{cav} = 8$ and 15 Å are shown in Figures 6 and 7, respectively. The value of the power spectrum, $\xi(\omega)$, decays quickly at low frequencies before slowing considerably around 500 cm^{-1}. This means the higher the solute vibrational frequency, the slower the vibrational energy relaxation. From the decomposition of $\xi(\omega)$, we see that for a solute with a low vibrational frequency both the vibration−rotation coupling and Coulombic interactions will have a sizable contribution to the vibrational energy relaxation time. At the AB$^-$ solute vibrational frequency (800 cm^{-1}, see the insets in Figures 6 and 7), the total power spectra are dominated by the Lennard-Jones interactions as seen also in the force TCF. Note that the vibration−rotation coupling in the smallest cavity (Figure 6) contributes a greater portion than in the larger cavities.

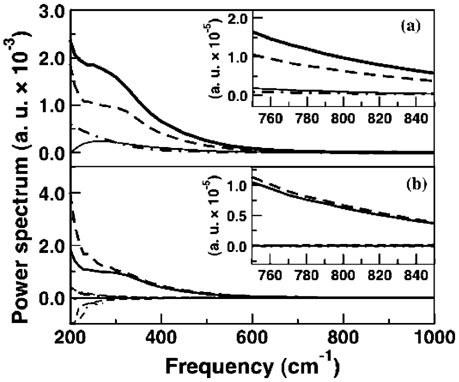

Figure 6. Decomposition of the power spectrum of the force correlation function for $R_{cav} = 8$ Å into components arising from different parts of the solute−solvent interaction. Shown in panel a are the total (thick solid line) along with the potential (dashed line), vibration−rotation coupling (dash−dotted line), and cross term (thin solid line) contributions. In panel b, the potential (thick solid line), Lennard-Jones (thick dashed line), Coulomb (thick dash−dotted line), and cavity wall (thin solid line) interaction contributions are shown along with the Lennard-Jones−Coulomb (thin dashed line), Lennard-Jones−wall (thin dash−dotted line), and Coulomb−wall (dot−dash-dashed line) cross terms. Enlargements near vibrational frequency $\omega_0 = 800$ cm^{-1} are shown in the insets.

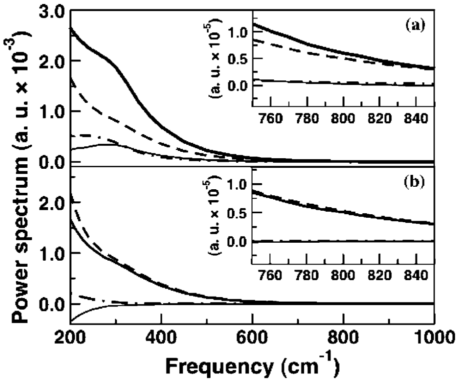

Figure 7. Same as Figure 6 except for $R_{cav} = 15$ Å. In panel b, contributions and cross terms related due to the cavity wall interactions are small and not shown.

C. Frequency Shift. We have calculated the solute frequency shift induced by the solvent according to eqs 8−10, and the average frequency shifts are listed in Table 3. The solute frequency is blueshifted from the gas-phase value for all cavities considered as well as the bulk. Overall, the dependence of the frequency shift on cavity size is not monotonic like that of T_1. The largest frequency blueshift (14.4 cm^{-1}) is found in the smallest cavity, while the smallest blueshift (2.9 cm^{-1}) is observed in the bulk system. However, due to a larger redshift (6.3 cm^{-1}) in the linear coupling term, eq 9, the smallest blueshift (3.7 cm^{-1}) among the cavity systems is found for $R_{cav} = 10$ Å, while the values for $R_{cav} = 12$−20 Å are all between 5 and 6 cm^{-1}.

To further analyze the mechanism of the frequency shift, we decompose the total frequency shift into components arising

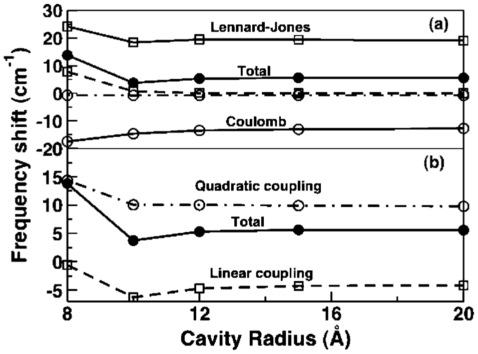

Figure 8. Decompositions of the solvent-induced frequency shift for cavities of varying size into components arising from different interactions. Shown in panel a are the total (filled circles, solid line), Lennard-Jones (open squares, solid line), Coulomb (open circles, solid line), vibration−rotation coupling (open circles, dot−dashed line), and cavity wall (open squares, dashed line) frequency shifts. Shown in panel b are the total (filled circles, solid line), linear coupling (open squares, dashed line), and quadratic coupling (open circles, dot−dashed line) frequency shifts.

from different potential terms: the solute vibration−rotation coupling and the Coulomb, Lennard-Jones, and cavity wall interactions. The results are presented in Table 3 and Figure 8. In addition, the linear (ω_1) and quadratic (ω_2) coupling terms have been separated (see Table 3 and Figure 8b). From Table 3, we can draw several conclusions. First, the total frequency shift is mainly determined by a large cancellation from the Lennard-Jones and Coulomb terms. The former gives a blueshift and the latter a redshift for all the systems studied. This implies that the Coulomb interactions are primarily attractive, while the Lennard-Jones interactions are primarily repulsive; since the total frequency shift is positive (blueshifted), the repulsive forces dominate. Second, the Coulomb force-induced redshift is 17.5 cm^{-1} for the smallest cavity and decreases monotonically to 12.7 and 12.5 cm^{-1} for the largest cavity and the bulk, respectively. However, the Lennard-Jones force-induced blueshift follows the same pattern, except for the $R_{\text{cav}} = 10$ Å cavity. We attribute the exceptionally small value (18.4 cm^{-1}) for the $R_{\text{cav}} = 10$ Å cavity to the relatively large change in solvent density when the solute moves between the solvent layers (see Figure 2). Third, the frequency shift due to the solute vibration−rotation coupling is essentially constant for all systems, consistent with eq 15. Fourth, except for the smallest cavity system (blueshifted by 7.7 cm^{-1}), the frequency shifts due to the cavity wall are very small (less than 1 cm^{-1}). Finally, the linear coupling term, eq 9, dominates over quadratic coupling, eq 10, for the frequency shift induced by the Coulomb and Lennard-Jones forces for all systems. However, for the total frequency shift the blueshift induced by the quadratic term is larger than the redshift induced by the linear term due to cancellations in the linear term between the different interactions. Similar behavior was also found by Hynes et al., who studied the frequency shift of CN$^-$ in water.[84]

It is interesting to note that the blueshift in the solute frequency is in accord with the results of Zhong et al. for N$_3^-$, NCO$^-$, and NCS$^-$ in nonionic and positively charged RMs.[5] They find redshifts for these ions in negatively charged RMs. However, they find in all cases that the magnitude of the shift diminishes as the RM size is increased in contrast to the present results. In the case of nonionic and positively charged RMs they find the bulk value for the solvent-induced frequency shift is not reached for the largest RM, which is consistent with our results.

D. Vibrational Dephasing Time. The vibrational dephasing times, T_2*, obtained as the integral of the frequency correlation function, eq 7, are given in Table 2. Unlike T_1, which increases monotonically with cavity size, there is an exceptionally long T_2* for the smallest cavity system. However, T_2* increases toward the bulk value, but does not reach it, as R_{cav} increases from 10 to 20 Å. The different trends for T_2* and T_1 indicate that different mechanisms are operative, or at least dominant, for energy and phase relaxation in these cavity systems. According to eq 8, we split the frequency correlation function into the contributions arising from the linear and quadratic coupling and the cross-correlation term:

$$\langle \delta\omega(t)\delta\omega(0)\rangle = \langle \delta\omega_1(t)\delta\omega_1(0)\rangle + \langle \delta\omega_2(t)\delta\omega_2(0)\rangle + 2\langle \delta\omega_1(t)\delta\omega_2(0)\rangle \quad (21)$$

Then $T_2{*}^{-1}$ is the integral of the sum of three contributions according to eq 7. Thus, while T_1 only involves the linear force, F_1, T_2* involves both linear and quadratic terms. Unlike the frequency shifts, for which quadratic coupling plays an important role, the dominant contribution to the dephasing time is from the $\delta\omega_1$ correlation function for all systems. As pointed out by Rey and Hynes[84] the negligible role of the $\delta\omega_2$ correlation function is due to two effects: the corresponding fluctuations are both small and short-lived. If we neglect the quadratic coupling contribution, and substitute eq 9 into eq 7, then the dephasing rate constant can be rewritten as

$$T_2{*}^{-1} \approx (Q_{11} - Q_{00})^2 \int_0^\infty \langle \delta F_1(t)\delta F_1(0)\rangle \, \mathrm{d}t \quad (22)$$

This implies that the dephasing time is related to the decay of the force autocorrelation function, especially the slow decay, which contributes strongly to the integral in eq 22. This is useful for investigating the dephasing mechanism (though the results in Table 2 are obtained from eq 7, the full expression). Recall that for the slow decay of the force TCF (Figure 3), the value at $t = 1$ ps decreases with increasing cavity size except for the smallest cavity. Since the short-time decay is similar, the dependence of the integral of the force correlation function ($T_2{*}^{-1}$) on R_{cav} can be predicted based on the value of the TCF at, for example, $t = 1$ ps. On the basis of Figure 3, this gives the correct result: T_2* is the shortest for $R_{\text{cav}} = 10$ Å and increases with cavity size toward the bulk value, while the value for the smallest cavity is comparatively long.

Since the slow decay process plays an important role in the dephasing time, we now return to the solute position distributions shown in Figure 2. It is useful to examine the time the solute spends in the high density solvent layers as a function of cavity size. To address this we have calculated the solute residence time in these layers from the time-dependent solute center-of-mass position in the NEMD simulations. The calculated solute residence time in a high density solvent layer is 195, 101, 132, 140, and 136 ps (over the total propagation time of 200 ps) for a cavity of radius 8, 10, 12, 15, and 20 Å, respectively. Thus, in the smallest cavity the solute is in the high local density solvent layer almost the entire time. In contrast, the solute residence time is shortest in the cavity with $R_{\text{cav}} = 10$ Å; the solute only spends half of the total time located in the solvent layers. The residence time is essentially the same for $R_{\text{cav}} = 12$, 15, and 20 Å while the local density in the layers decreases as R_{cav} increases. Interestingly, T_2* is 20 times *shorter* for $R_{\text{cav}} = 10$ Å compared to 8 Å and increases continuously for the larger cavities. Since T_2* is short compared to the residence times, it appears that the overall dephasing time is a result of an average over an inhomogeneous distribution of solute positions. Further, for the smallest cavities, the larger the residence time in the high-density regions the longer T_2*; however, for the larger cavities the residence time is constant while the solvent density becomes more homogeneous and T_2* increases as R_{cav} increases. One possible explanation for this observation is that the long-time tail of the force autocorrelation function is determined predominantly when the solute is in a lower density region. Thus, for the smallest cavities there is a direct relationship between T_2* and the residence time while for the largest three cavities ($R_{cav} = 12$, 15, and 20 Å), for which the residence time is essentially constant, the density in the regions between solvent layers increases with R_{cav}, thereby lengthening the dephasing time.

It is worth noting that, due to the confinement effect, even for the largest cavity size we studied, the solvent still has a weakly layered structure with somewhat higher density than the bulk system. Therefore, as for T_1 and the frequency shifts the vibrational dephasing time, T_2*, does not reach the value for the bulk system for the largest cavity considered here.

The results for the simple model considered here are in qualitative agreement with experimental measurements of dephasing in neat solvents confined in sol−gels (for example, by Jonas and co-workers and Tominaga et al.) who found that the dephasing time decreases with increasing confinement.[1−3,48,49] Two key differences are (1) the experiments observe a monotonic trend, and (2) they generally find that $T_2^{-1} \propto 1/R_{cav}$ (which we do not). These differences may be attributable to (1) the smallest cavity we have studied (which accounts for the nonmonotonic behavior) is significantly smaller than the sol−gel pores considered experimentally, and (2) the experiments consider dephasing of a neat solvent rather than a single solute and thus are sensitive to the number of solvent molecules near the pore surface which may account for the $T_2^{-1} \propto 1/R_{cav}$ relationship. It is interesting to note that the experiments of Zhong et al. in aqueous RMs find, in contrast to the measurements in sol−gels and the present results, a dephasing time for a single anionic solute that is roughly independent of the water pool size (based on the line widths of the infrared spectra).[6,7] Thus, the cavity wall interactions and solvent properties (e.g., hydrogen-bonding) clearly affect the dephasing, and we are currently investigating these effects.

Concluding Remarks

We have calculated the VER times for a model anion solute in a CH_3I solvent confined in cavities of varying size as well as the bulk system using EMD and NEMD simulations. The results show that T_1 for the confined systems is smaller than the bulk value, and increases with cavity size but does not reach the bulk value for the largest cavity considered ($R_{cav} = 20$ Å). We attribute the changes in T_1 to the presence of high local density solvent layers induced by the confinement. In these solvent layers, the repulsive, Lennard-Jones forces play an important role and the enhancement of the local density leads to faster vibrational energy relaxation.

The good agreement between EMD and NEMD calculations of T_1 supports the trend found for the VER time with cavity size. On the other hand, comparing the NEMD simulations with EMD simulations including and excluding the solute vibration−rotation coupling contribution demonstrates that this term is important for the systems studied.

On the basis of an analysis of the force TCF, we conclude that the primary contribution to the TCF is the Lennard-Jones interaction. On the other hand, direct contributions from the Coulomb and cavity wall interactions are not important for the these systems (rigid wall, hydrophobic cavities). The Coulombic contribution to T_1 is likely through an indirect mechanism discussed previously by Ladanyi et al.[83] They found that although the Coulomb force may not directly provide the principal force acting along the vibrational bond the presence of a strong electrostatic potential creates equilibrium configurations conducive to rapid relaxation by increasing the solute−solvent non-Coulombic forces.

The solvent-induced frequency shifts have been calculated by perturbation theory including up to quadratic coupling in the solute−solvent interaction. The quadratic coupling induces a blueshift in the solute frequency relative to the gas-phase value, while the linear coupling gives a redshift. However, the former dominates, giving a blueshift in the solute frequency for all cavity sizes. On the other hand, if the frequency shift is split into components arising from different solute−solvent interactions, the short-range Lennard-Jones interactions contribute a large blueshift while the longer-range Coulomb interactions give a large redshift. The total blueshift results from strong cancellation in these terms. The vibration−rotation coupling contribution to the frequency shifts is independent of the surroundings and the cavity wall contribution is significant only for the smallest cavity.

We have calculated the vibrational dephasing time T_2* for the cavity systems as well as the bulk. Unlike T_1, which is controlled by the fast decay process of the force TCF, the vibrational dephasing time in the cavities is controlled by the long-time decay of the force correlation function. We note that except for the smallest cavity the confinement effects on the frequency shift and T_2^{*-1} follow trends similar to experimental observations for porous sol−gels.[1−3,9,10,48,49] However, since the simple rigid spherical cavity model used here does not involve a strong surface interaction, primarily geometrical confinement effects are considered in the present simulations. Thus, the present results indicate that strong solvent-surface interactions are not a requirement for a decrease in T_2* with decreasing R_{cav}; we attribute the trend in this model system to the increasing local solvent density experienced by the solute as the cavity size is reduced. We do not find a linear dependence of T_2* on R_{cav} as has been observed in experiments on neat confined solvents. We believe this may be related to the fact that dephasing of a single solute has been examined here whereas the experiments have probed dephasing of neat solvents which are sensitive to the number of molecules near the surface.

The results of the present calculations clearly show that confining the solvent strongly affects the vibrational dynamics. The simplicity of the model system used in the present work implies that the trends with cavity size are primarily a result of solvent confinement alone (e.g., changes in the solvent local density, solute position, and solute dynamics). Thus, this study represents a first step in elucidating the mechanisms of confinement effects on vibrational dynamics and the origins of the trends in VER, dephasing, and frequency shifts with the confinement length scale(s). The exploration of additional cavity characteristics such as dimensionality, surface chemistry, and flexibility as well as solvent properties (e.g., hydrogen bonding) will be required in order to successfully model experimental results (which themselves display differing trends); this is the subject of work currently underway.

Acknowledgment. We would like to thank Dr. Jeff C. Owrutsky for several useful discussions. This work was supported by the Chemical Sciences, Geosciences and Biosciences

Division, Office of Basic Energy Sciences, Office of Science, U.S. Department of Energy.

References and Notes

(1) Korb, J.-P.; Delville, A.; Xu, S.; Demeulenaere, G.; Costa, P.; Jonas, J. *J. Chem. Phys.* **1994**, 7074.

(2) Czeslik, C.; Kim, Y. J.; Jonas, J. *J. Raman Spectrosc.* **2000**, *31*, 571.

(3) Yi, J.; Jonas, J. *J. Phys. Chem.* **1996**, *100*, 16789.

(4) Thompson, W. H. *J. Chem. Phys.* **2002**, *117*, 6618.

(5) Zhong, Q.; Steinhurst, D. A.; Carpenter, E. E.; Owrutsky, J. C. *Langmuir* **2002**, *18*, 7401.

(6) Zhong, Q.; Baronavski, A. P.; Owrutsky, J. C. *J. Chem. Phys.* **2003**, *118*, 7074.

(7) Zhong, Q.; Baronavski, A. P.; Owrutsky, J. C. *J. Chem. Phys.* **2003**, *119*, 9171.

(8) Faeder, J.; Ladanyi, B. M. *J. Phys. Chem. B* **2000**, *104*, 1033.

(9) Kalampounias, A. G.; Yannopoulos, S. N.; Steffen, W.; Kirillova, L. I.; Kirillov, S. A. *J. Chem. Phys.* **2003**, *118*, 8340.

(10) Kalampounias, A. G.; Kirillov, S. A.; Steffen, W.; Yannopoulos, S. N. *J. Mol. Struct.* **2003**, *651−653*, 475.

(11) Senapati, S.; Chandra, A. *J. Chem. Phys.* **1999**, *111*, 1223.

(12) Senapati, S.; Berkowitz, M. L. *J. Chem. Phys.* **2003**, *118*, 1937.

(13) Hadjiagapiou, I. A. *Phys. Rev. E* **2002**, *65*, 021605.

(14) Zhang, L.; Davis, H. T.; Kroll, D. M. *J. Phys. Chem.* **1995**, *99*, 2878.

(15) Israelachvili, J. N. *Intermolecular and Surface Forces*; Academic: New York, 1992.

(16) Baumann, R.; Ferrante, C.; Kneuper, E.; Deeg, F.-W.; Braeuchle, C. *J. Phys. Chem. A* **2003**, *107*, 2422.

(17) Baumann, R.; Ferrante, C.; Deeg, F. W.; Brauchle, C. *J. Chem. Phys.* **2001**, *114*, 5781.

(18) Das, K.; Sarkar, N.; Das, S.; Datta, A.; Bhattacharyya, K. *Chem. Phys. Lett.* **1996**, *249*, 323.

(19) Sarkar, N.; Das, K.; Datta, A.; Das, S.; Bhattacharyya, K. *J. Phys. Chem.* **1996**, *100*, 10523.

(20) Sarkar, N.; Datta, A.; Das, S.; Bhattacharyya, K. *J. Phys. Chem.* **1996**, *100*, 15483.

(21) Pal, S. K.; Sukul, D.; Mandal, D.; Sen, S.; Bhattacharyya, K. *J. Phys. Chem. B* **2000**, *104*, 2613.

(22) Datta, A.; Pal, S. K.; Mandal, D.; Bhattacharyya, K. *J. Phys. Chem. B* **1998**, *102*, 6114.

(23) Sen, S.; Sukul, D.; Dutta, P.; Bhattacharyya, K. *J. Phys. Chem. A* **2001**, *105*, 10635.

(24) Pant, D.; Riter, R. E.; Levinger, N. E. *J. Chem. Phys.* **1998**, *109*, 9995.

(25) Pant, D.; Levinger, N. E. *Langmuir* **2000**, *16*, 10123.

(26) Riter, R. E.; Kimmel, J. R.; Undiks, E. P.; Levinger, N. E. *J. Phys. Chem. B* **1997**, *101*, 8292.

(27) Riter, R. E.; Willard, D. M.; Levinger, N. E. *J. Phys. Chem. B* **1998**, *102*, 2705.

(28) Riter, R. E.; Undiks, E. P.; Kimmel, J. R.; Levinger, N. E. *J. Phys. Chem. B* **1998**, *102*, 7931.

(29) Riter, R. E.; Undiks, E. P.; Levinger, N. E. *J. Am. Chem. Soc.* **1998**, *120*, 6062.

(30) Willard, D. M.; Riter, R. E.; Levinger, N. E. *J. Am. Chem. Soc.* **1998**, *120*, 4152.

(31) Willard, D. M.; Levinger, N. E. *J. Phys. Chem. B* **2000**, *104*, 11075.

(32) Hazra, P.; Sarkar, N. *Chem. Phys. Lett.* **2001**, *342*, 303.

(33) Hazra, P.; Chakrabarty, D.; Sarkar, N. *Chem. Phys. Lett.* **2002**, *358*, 523.

(34) Korb, J.-P.; Cros, F.; Xu, S.; Malier, L.; Jonas, J. *J. Chem. Phys.* **1997**, *107*, 4044.

(35) Korb, J. P.; Xu, S.; Jonas, J. *J. Chem. Phys.* **1993**, *98*, 2411.

(36) Korb, J.-P.; Malier, L.; Cros, F.; Xu, S.; Jonas, J. *Phys. Rev. Lett.* **1996**, *77*, 2312.

(37) Zhang, J.; Jonas, J. *J. Phys. Chem.* **1993**, *97*, 8812.

(38) Farrer, R. A.; Fourkas, J. T. *Acc. Chem. Res.* **2003**, *36*, 605.

(39) Loughnane, B. J.; Fourkas, J. T. *J. Phys. Chem. B* **1998**, *102*, 10288.

(40) Loughnane, B. J.; Farrer, R. A.; Scodinu, A.; Fourkas, J. T. *J. Chem. Phys.* **1999**, *111*, 5116.

(41) Loughnane, B. J.; Scodinu, A.; Fourkas, J. T. *J. Phys. Chem. B* **1999**, *103*, 6061.

(42) Loughnane, B. J.; Farrer, R. A.; Scodinu, A.; Reilly, T.; Fourkas, J. T. *J. Phys. Chem. B* **2000**, *104*, 5421.

(43) Loughnane, B. J.; Scodinu, A.; Fourkas, J. T. *Chem. Phys.* **2000**, *253*, 323.

(44) Streck, C.; Mel'nichenko, Y. B.; Richert, R. *Phys. Rev. B* **1996**, *53*, 5341.

(45) Richert, R. *Phys. Rev. B* **1996**, *52*, 15762.

(46) Datta, A.; Mandal, D.; Pal, S. K.; Bhattacharyya, K. *J. Phys. Chem. B* **1997**, *101*, 10221.

(47) Bhattacharyya, K. *J. Mol. Liq.* **1993**, *57*, 115.

(48) Wallen, S. L.; Nikiel, L.; Yi, J.; Jonas, J. *J. Phys. Chem.* **1995**, *99*, 15421.

(49) Tominaga, K.; Okuno, H.; Maekawa, H.; Tomonaga, T.; Loughname, B. J.; Scodinu, A.; Fourkas, J. T. In *Liquid Dynamics: Experiment, Simulation, and Theory*; Fourkas, J. T., Ed.; The American Chemical Society: Washington, DC, 2002; Vol. 820; p 160.

(50) Horikawa, S.; Itoh, H.; Tabata, J.; Kawamura, K.; Hondoh, T. *J. Phys. Chem. B* **1997**, *101*, 6290.

(51) van Klaveren, E. P.; Michels, J. P. J.; Schouten, J. A.; Klug, D. D.; Tse, J. S. *J. Chem. Phys.* **2002**, *117*, 6637.

(52) Klafter, J.; Blumen, A.; Drake, J. M. *Relaxation and Diffusion in Restricted Geometries*, in *Molecular Dynamics in Restricted Geometries*; Wiley & Sons: New York, 1989.

(53) Landau, L.; Teller, E. *Z. Sowjetunion* **1936**, *10*, 34.

(54) Whitnell, R. M.; Wilson, K. R.; Hynes, J. T. *J. Phys. Chem.* **1990**, *94*, 8625.

(55) Whitnell, R. M.; Wilson, K. R.; Hynes, J. T. *J. Chem. Phys.* **1992**, *96*, 5354.

(56) Bader, J. S.; Berne, B. J. *J. Chem. Phys.* **1994**, *100*, 8359.

(57) Skinner, J. L.; Park, K. *J. Phys. Chem. B* **2001**, *105*, 6716.

(58) Kim, H.; Rossky, P. J. *J. Phys. Chem. B* **2002**, *106*, 8240.

(59) Egorov, S. A.; Everitt, K. F.; Skinner, J. L. *J. Phys. Chem. A* **1999**, *103*, 9494.

(60) Miller, D. W.; Adelman, S. A. *J. Chem. Phys.* **2002**, *117*, 2672.

(61) Egorov, S. A.; Skinner, J. L. *J. Chem. Phys.* **1996**, *105*, 7047.

(62) Li, S.; Thompson, W. H. *Chem. Phys. Lett.* **2004**, *383*, 326.

(63) Rostkier-Edelstein, D.; Graf, P.; Nitzan, A. *J. Chem. Phys.* **1997**, *107*, 10470.

(64) Hurwitz, H., Jr.; Zweifel, P. F. *Mathematical Tables and Aids to Computation* **1956**, *10*, 140.

(65) Thakkar, A. J.; Smith Jr, V. H. *Comput. Phys. Commun.* **1975**, *10*, 73.

(66) Clenshaw, C. W.; Curtis, A. R. *Numer. Math.* **1960**, *2*, 197.

(67) National Physical Laboratory. *Modern Computing Methods*, 2nd ed.; H.M.S.O.: London, 1961.

(68) Tuckerman, M.; Berne, B. J. *J. Chem. Phys.* **1993**, *98*, 7301.

(69) Kubo, R. *Adv. Chem. Phys.* **1963**, *13*, 101.

(70) Kubo, R. *J. Math. Phys.* **1963**, *4*, 174.

(71) Kubo, R. *Fluctuations, Relaxation, and Resonance in Magnetic Systems*, Ter Haar, D., Ed.; Plenum: New York, 1962.

(72) Oxtoby, D. W. *J. Chem. Phys.* **1978**, *68*, 5528.

(73) Everitt, K. F.; Skinner, J. L. *J. Chem. Phys.* **2001**, *115*, 8531.

(74) Linse, P. *J. Chem. Phys.* **1989**, *90*, 4992.

(75) Linse, P.; Halle, B. *Mol. Phys.* **1989**, *67*, 537.

(76) Allen, M. P.; Tildesley, D. J. *Computer Simulation of Liquids*; Oxford: Oxford, England, 1987.

(77) Freitas, F. F. M.; Fernands, F. M. S. S.; Cabral, B. J. C. *J. Phys. Chem.* **1995**, *99*, 5180.

(78) Gayathri, N.; Bhattacharyya, S.; Bagchi, B. *J. Chem. Phys.* **1997**, *107*, 10381.

(79) Oxtoby, D. W. *Adv. Chem. Phys.* **1981**, *47*, 487.

(80) Nose, S. *J. Chem. Phys.* **1984**, *81*, 511.

(81) Hoover, W. G. *Phys. Rev. A* **1985**, *31*, 1695.

(82) Smith, W.; Forester, T. R. DLPOLY; 2.13 ed.; CCLRC, Daresbury Laboratory, Daresbury, England, 2002.

(83) Ladanyi, B. M.; Stratt, R. M. *J. Chem. Phys.* **1999**, *111*, 2008.

(84) Rey, R.; Hynes, J. T. *J. Chem. Phys.* **1998**, *108*, 142.

(85) Shoemarker, D. P.; Garland, C. W.; Nibler, J. *Experiments in Physical Chemistry*, 5th ed.; McGraw-Hill: New York, 1989.